Highlights

Characterizing Long-term Cosmic Ray Time Series with Geometric Network Curvature Metrics

D. Sierra-Porta

- Complex networks reveal cosmic ray patterns across neutron monitoring stations.
- Forman-Ricci curvature links magnetic rigidity and cosmic ray variability.
- Ricci Flow highlights inverse relationship with neutron detector geomagnetic rigidity cutoff.

Characterizing Long-term Cosmic Ray Time Series with Geometric Network Curvature Metrics

D. Sierra-Porta[a]

[a]Universidad Tecnológica de Bolívar, Facultad de Ciencias Básicas, Parque Industrial y Tecnológico Carlos Vélez Pombo Km 1 Vía Turbaco, 130010, Cartagena de Indias, Colombia

Abstract

This study investigates the relationship between geometry and nonlinear dynamics in time series of cosmic ray counts recorded at neutron monitors at ground stations. Using advanced geometric and topological analysis techniques, we construct complex networks from the time series and calculate curvature measures such as Ollivier-Ricci curvature, Forman-Ricci curvature, and Ricci flow for each series. The analysis reveals significant correlations between these curvature metrics and key parameters such as geomagnetic cutoff rigidity and detector latitude. In particular, Forman-Ricci curvature exhibits a robust negative correlation with cutoff rigidity (Pearson $r = -0.85$, Spearman $\rho = -0.86$, p-value$< 10^{-5}$), while Ricci flow also shows a strong and highly significant inverse relationship with cutoff rigidity (Pearson $r = -0.92$, Spearman $\rho = -0.89$, p-value$< 10^{-7}$). These results suggest that the geometrical structure of the networks, influenced by geomagnetic conditions, plays a crucial role in the variability, complexity, and fractality of cosmic ray time series. Furthermore, the study underscores the importance of considering network topology and curvature metrics in the analysis of cosmic ray data, offering new perspectives for understanding space weather phenomena and improving predictive models. This integrative approach not only advances our knowledge of cosmic ray dynamics, but also has important implications for mitigating risks associated with space weather conditions on Earth.

Keywords: Geomagnetic Rigidity Cutoff, Cosmic Rays, Space Weather, Topological Data Analysis

1. Introduction

Cosmic rays (CRs) (Grieder, 2001; Ziegler, 1996), consisting mainly of protons and atomic nuclei, are high-energy (10^6–10^{20} eV) charged particles that constantly bombard the Earth's atmosphere from outer space. They originate from extremely energetic events in the universe, such as supernova explosions and coronal mass ejections from the Sun. As these particles collide with the Earth's atmosphere, they trigger cascades of secondary particles—including neutrons, muons, and electrons—which can be detected by sensitive instruments on the Earth's surface and in space (Tatischeff et al., 2021).

The characterization of CRs is fundamental to understanding their impact on various aspects of life on Earth and modern technology. CRs are closely related to space weather, as variations in their flux can influence solar activity and near-Earth space weather (Dorman, 2021; Guhathakurta, 2021). These effects can have significant implications for ground-based technology (Simonsen et al., 2020), including satellite navigation systems such as GPS, orbiting satellites (Höeffgen et al., 2020; Köksal et al., 2021), radio communications, and mobile communications networks (Sharma and Lamba, 2017). Furthermore, CRs can affect human health (Singh et al., 2011), especially at high altitudes where exposure to cosmic radiation is higher, affecting air flight and manned space missions (Lim, 2002; Cucinotta and Durante, 2006).

Previous studies have analyzed CRs time series in relation to various contributions in several emerging fields seeking additional insight. For example, Sierra-Porta (2022) investigated the fractal properties of CRs and their cross-correlations with solar dynamics. The study examined CRs measurements obtained by a neutron monitoring station in Moscow, along with ten heliospheric parameters, including sunspots, solar activity rates, Alfven number, geomagnetic storm rates, proton temperature, and interplanetary magnetic field magnitude. Using multifractal detrended cross-correlation analysis (MFDCCA) (Zhou, 2008), the study identified positive long-term correlations with multifractal behavior in CRs time series and the heliospheric parameters, implying effective correlations between cosmic radiation and space weather, particularly in relation to the dynamics of the interplanetary medium (Kudela and Venkatesan, 1995; Gopinath and Prince, 2017).

Geomagnetic Cutoff Rigidity (R_c), a critical measurement in CRs detection, is intricately related to the geographic latitude of CRs detectors. This rigidity refers to the minimum amount of linear momentum that a charged particle must possess to penetrate the Earth's atmosphere and be detected by a surface detector. Essentially, R_c represents the energy threshold below which cosmic particles cannot reach the Earth's surface, being deflected by the Earth's magnetic field. The value of R_c depends on both the strength and orientation of the Earth's magnetic field at the detector location, leading to significant variations based on latitude. Generally, the Earth's geomagnetic cutoff rigidity is higher at lower latitudes (around the equator), effectively deflecting lower-energy particles more efficiently, and decreases toward the poles, where more low-energy cosmic rays can penetrate (Herbst et al., 2013; Smart and Shea, 2005; Danilova et al., 2023; Comedi et al., 2020; Gerontidou et al., 2021). This variation in R_c is closely tied to the geometry of Earth's magnetic field and has significant implications for cosmic ray detection at different latitudes.

A recent study explored the relationship between CRs intensities and cutoff rigidity through multifractal detrended fluctuation analysis (MFDFA) (Sierra-Porta and Domínguez-Monterroza, 2022; Kantelhardt et al., 2002). The research investigated how magnetic cutoff rigidity relates to variability and multifractal behavior in CRs flux time series detected by neutron monitors on Earth's surface. Since R_c is strongly dependent on the geographical latitude of the detectors, not all detectors record the same number of CRs counts (see also: Giri et al. (2024) and Yu et al. (2009)). The study's findings suggest a bias in the chaotic nature of the CRs series associated with the latitude of the monitoring stations. A significant relationship was established between R_c, the behavior variations, and the Hurst exponent of the series corresponding to the counts at the neutron monitoring stations. Notably, an inverse relationship was observed, where a higher R_c correlates with a lower Hurst exponent, highlighting how geographical and geomagnetic factors interplay in CRs monitoring.

A recent study by Sierra-Porta (2024) examined the relationship between R_c and chaotic behavior in CRs time series using visibility graph analysis (VGA) (Stephen et al., 2015; Lacasa and Toral, 2010) and network analysis techniques. In this study, the time series of CRs flux measured by neutron detectors at 16 monitoring stations distributed worldwide were analyzed. By applying visibility graph analysis, the relationship between geomagnetic cutoff rigidity and fractality exhibited by the CRs time series topology was explored. The results revealed a significant association between R_c and CRs time series fractality. Specifically, the analysis of visibility graphs and network properties of time series identified a relationship between R_c and fractality, providing insights into the chaotic nature of CRs variations and their potential applications for predictability.

A recent study investigated Forbush Decrease (FD) events across different solar cycles and examined their correlation with geomagnetic storm conditions using multifractal detrended fluctuation analysis (Sierra-Porta, 2024). In that work, the amplitude of the multifractal spectrum was compared between FD series associated with stronger geomagnetic storms (maximum storm index exceeding 6) and those linked to weaker or negligible storms. It was found that FD series falling under the stronger storm category exhibited a notably greater spectrum amplitude, suggesting that the fractal complexity of these events is closely tied to the severity of geomagnetic activity. This finding underscores the importance of geometric and topological approaches in shedding light on the intricate interplay between cosmic ray phenomena and space weather conditions.

In addition, it is important to highlight the growing interest in the analysis of network geometry, a field that has experienced a remarkable boom in recent times. Network geometry focuses on the study of the geometric and topological properties of complex networks, which can represent a wide variety of dynamic systems and relationships between interconnected entities (Boguna et al., 2021; Mulder and Bianconi, 2018; Salanti et al., 2008). This approach has found applications in various fields, including finance (Samal et al., 2021; Yen et al., 2021), wireless communications (Haenggi, 2012), epidemic studies (de Souza et al., 2021), and time series analysis of biological and social systems (Albert et al., 2014). In finance, network geometry is used to analyze the interconnectedness between financial institutions and predict the propagation of systemic risks (Marti et al., 2021; Yen et al., 2021; Granados and Vargas, 2022). In economics, it is used to study the structure of trade and collaboration networks between countries. In time series analysis, network geometry provides tools to visualize and analyze the time evolution of complex dynamic systems. This innovative approach has opened new perspectives for understanding the complexity inherent in a wide range of phenomena, from economic interactions to climate dynamics, and its application in signal and data network analysis continues to be an active and promising area of research.

The relationship between curvature measures with chaos and nonlinear dynamics is established through differential geometry, topology, and dynamical systems theory (Donner et al., 2011). In nonlinear dynamical systems, chaos can arise due to sensitivity to initial conditions and bifurcations in system behavior. Curvature measurements and Ricci flow can provide information on how the geometry and topology of the network influence the sensitivity to initial conditions and the occurrence of bifurcations (Baptista et al., 2023; Jin, 2013; Golubitsky and Stewart, 2015).

Moreover, chaos is often associated with fractal structures and fractal dimensions in the phase space of a dynamical system. Curvature measurements and Ricci flow can help characterize the fractal geometry of the lattices or varieties associated with the dynamical system, providing information about the complexity and fractal nature of the system (El-Nabulsi, 2022; de Souza et al., 2021). Finally, there are theoretical connections between chaos theory and complex network theory. Curvature measures and Ricci flow can be used to characterize the structure and dynamics of complex networks, providing insight into how chaotic phenomena emerge in complex interconnected systems.

In this contribution, we explore the importance of understanding variations and characterizations of CRs and their impact on space weather, ground-based technology, and human life related topic. The focus of this study is on investigating the relationship between CRs intensity dynamics and the geometric structure of networks constructed from time series of CRs counts. This study use geometric and topological analysis techniques to examine how the geometry of these networks influences the variability of CRs counts and provide a new perspective to understand the complexity of these cosmic phenomena and their impact on our terrestrial environment. Specifically, we will employ advance methods of topological and network geometry analysis, focusing on features derived from the network's Ricci curvatures and Ricci flow, to provide insights from a unique viewpoint concerning the relationships identified in previous studies.

2. Data available

The data used in this study came from two main sources. First, data on CRs count intensities were obtained from the Institute of Terrestrial Magnetism, Ionosphere and Pushkov Radio Wave Propagation of the Russian Academy of Sciences (IZMIRAN, `https://www.izmiran.ru/`) (Gaidash et al., 2017) which is a scientific institution founded in 1939 and has been engaged in research in the field of terrestrial magnetism, ionosphere and radio wave propagation. In addition, data from the Neutron Monitor Database (NMDB, `https://www.nmdb.eu/`), a real-time database for high-resolution neutron monitor measurements (Mavromichalaki et al., 2010, 2011), were used. NMDB provides access to neutron monitor measurements from stations around the world and aims to provide easy access to all neutron monitor measurements through a user-friendly interface. It is important to note that the data retrieved through NMDB are the property of the individual data providers and are free for non-commercial use within the restrictions imposed by the providers.

The data consist of cosmic ray count intensities recorded by neutron monitoring stations located across the globe. For this study, observations collected during solar cycle 24 (2008–2019) were used, ensuring that the selected time-frame included the largest possible number of stations without significant gaps in their respective datasets. By choosing this interval, it was possible to minimize missing data and reduce the need for imputation methods, thereby preserving the integrity of the original measurements. Each record represents the amount of cosmic rays detected by a station in a specific time interval, enabling an examination of the temporal variability of cosmic ray intensity during this solar cycle.

It is important to note that both the IZMIRAN database and the NMDB database contain measurements of CRs count intensities from multiple neutron monitoring stations distributed around the world. However, some of these stations may have missing data due to malfunction or because they are no longer operational. Therefore, as part of the data preparation process, a selection of stations retaining less than 5% missing data was made. This selection ensures the integrity of the data used in the study.

In this study, the time series were originally available in various temporal resolutions, ranging from 5-minute to monthly data. To maintain consistency across all stations and to concentrate on long-term trends, each dataset has been resampled to a one-month average. This approach effectively excludes short-scale events such as Forbush decreases, which often arise from coronal mass ejections, as well as variations related to corotating interaction regions (on timescales of the solar rotation period), ensuring that only longer-term cosmic ray modulations are captured. Consequently, this methodology highlights the contribution of solar cycle variations in the heliospheric magnetic field to cosmic ray dynamics, rather than transient or local phenomena. Additionally, the monthly aggregation helps reduce computational overhead and simplifies comparisons across stations. Still, the raw data at higher resolutions (hourly or finer) remain available for any future study aimed at investigating short-lived or more event-specific effects.

Additionally, a data engineering process was carried out to standardize and correct the data, as well as to build a complete database from the two original sources. This process included the integration of variables related to the height, latitude, longitude and country of location of each neutron monitoring station. These additional variables provide important contextual information that may be relevant for data analysis and interpretation of the results.

Table 1, shows the neutron monitors considered in this study specifying their localization, latitude, longitude, geomagnetic cutoff rigidity and altitude.

Table 1: Comparative characteristics of 22 neutron monitor data used in this study. Columns in table refer to Monitor (code name of the instrument used in this study), Lat (geographic latitude measured north), Lon (geographical longitude measured east), Alt (altitude measured in meters above sea level) and R_c at monitor station localization).

No.	Name, Loc	Monitor	Lat	Lon	Alt	R_c	Operated by
1	Barentsburg, Spitzbergen/PGIA	BRBG	78.07	14.21	51	0.01	Polar Geophysical Institute
2	Mirny, Antarctica/Russia	MRNY	66.55	93.01	30	0.03	Pushkov Institute of Terrestrial Magnetism
3	Inuvik, Canada/Bartol	INVK	68.36	133.72	21	0.30	Bartol Research Institute
4	Fort Smith, Canada/Bartol	FSMT	60.02	111.93	180	0.30	Bartol Research Institute
5	Thule, Greenland/Bartol	THUL	76.55	68.70	26	0.30	Bartol Research Institute
6	Nain, Canada/Bartol	NAIN	56.55	61.68	46	0.30	Bartol Research Institute
7	Apatity, Russia	APTY	67.57	33.40	181	0.65	Polar Geophysical Institute
8	SANAE, Antarctica	SNAE	71.67	2.85	865	0.73	South African National Antarctic Programme
9	Oulu, Finland	OULU	65.05	25.47	15	0.80	Sodankyla Geophysical Observatory
10	Kerguelen, Antarctica/France	KERG	49.35	70.25	33	1.14	French polar institute
11	Newark, USA/Bartol	NEWK	39.68	75.75	50	2.40	Bartol Research Institute
12	Moscow, Russia	MOSC	55.47	37.32	200	2.43	Pushkov Institute of Terrestrial Magnetism
13	Irkutsk2, Russia	IRK2	52.28	104.27	2000	3.64	Institute of Solar-Terrestrial Physics Russian Academy of Sciences
14	Lomnický štít, Slovakia	LMKS	49.20	20.22	2634	3.84	Institute of Experimental Physics, Košice, Slovakia
15	Jungfraujoch NM64, Switzerland	JUNG1	46.55	7.98	3570	4.50	Physikalisches Institut of the University of Bern
16	Jungfraujoch IGY, Switzerland	JUNG	46.55	7.98	3570	4.50	Physikalisches Institut of the University of Bern
17	Hermanus, South Africa	HRMS	34.43	19.23	26	4.58	South African National Space Agency
18	Baksan, Russia	BKSN	43.28	42.69	1700	5.60	Institute of Nuclear Physics Russian Academy of Sciences
19	Almaty, Kazakhstan	AATB	43.25	76.92	3340	6.69	Institute of Physics and Technology in Almaty, Kazakhstan
20	Mexico City, Mexico	MXCO	19.33	99.18	2280	8.20	Geophysical Institute, National Autonomous University of Mexico
21	Tsumeb, Namibia	TSMB	19.20	17.60	1240	9.29	Geological Survey of Namibia
22	Doi Inthanon, Thailand	PSNM	18.59	98.49	2565	16.80	Mahidol University, Chulalongkorn University

3. Materials and methods: Network geometry

Network geometry is an interdisciplinary field that focuses on the study of the geometric and topological properties of complex networks (Boguna et al., 2021). These networks can represent a wide range of dynamic systems and relationships between interconnected entities, and their analysis provides crucial information about the structure and dynamics of these systems. In recent years, network geometry has experienced increasing interest due to its ability to address a variety of problems in fields as diverse as physics, biology, computer science, and the social sciences.

In this study, we focus on three key curvature measures in network analysis: Ollivier-Ricci curvature, Forman-Ricci curvature, and Ricci flow. These measures provide invaluable information about the intrinsic geometry of networks and have proven to be particularly useful in characterizing the structure and dynamics of complex systems.

Given that we have established geometry applied to topological networks as a potent methodology for information extraction, one of our initial tasks with the dataset is constructing a network from each time series using a visibility graph analysis algorithm. Consequently, each time series corresponds to a network. Subsequently, we analyze each constructed network and compute two types of curvatures: Ollivier-Ricci curvature and Forman-Ricci curvature. As we are transitioning from a continuous object (time series) to a discrete one (network), curvature concepts can be utilized seamlessly. Moving forward, we apply two distinct types of discrete Ricci curvatures to CRs counting networks across various latitudes globally. Their definitions and applications are extensively documented in relevant literature. Discrete Ricci curvature provides valuable insights into network structure, making it highly relevant for both Network Science and Machine Learning. By connecting with numerous established network metrics and analytical approaches (Weber et al., 2017), it has been employed to investigate network data across a variety of domains, including biological (Tannenbaum et al., 2015; Weber et al., 2017; Sandhu et al., 2015), chemical (Leal et al., 2021), and financial transaction networks (Sandhu et al., 2016). In Machine Learning, discrete curvature has been leveraged to alleviate oversquashing in Graph Neural Networks (Topping et al., 2021; Nguyen et al., 2023) and to guide the selection of embedding spaces for Representation Learning (Weber, 2020). For completeness, we briefly outline their definitions here.

Ricci-curvature, for example, quantifies the intrinsic curvature of a network at each of its nodes, making it possible to identify regions of high curvature that may play a crucial role in network connectivity. On the other hand, the Forman-curvature provides an alternative measure of curvature that takes into account both the geometry and the topology of the network, allowing it to capture important features of its structure.

Taken together, these curvature measures offer a unique perspective for understanding the complexity of networks and their dynamic behavior. In this study, we will explore how these measures can be applied to the time series analysis of CRs counts and how they can provide relevant information about the dynamics and structure of these complex systems.

3.1. Ollivier-Ricci curvature

Consider a graph or network $G = (V, E)$, where V denotes the set of vertices and E the set of edges. To define Ollivier-Ricci curvature, we utilize the framework proposed by Ollivier (2009, 2007), which is based on the concept of optimal transport of probability measures between graph vertices.

Define a probability distribution over the vertex set $V(G)$. For a vertex $x \in V$, the probability measure $m_x^\alpha : V \to [0, 1]$ is defined as follows:

$$m_x^\alpha(v) = \begin{cases} \alpha & \text{if } v = x, \\ \frac{1-\alpha}{\deg(x)} & \text{if } v \text{ is a neighbor of } x, \\ 0 & \text{otherwise.} \end{cases} \tag{1}$$

Here, $\deg(x)$ represents the degree of vertex x, and $\alpha \in [0, 1]$ is a parameter that modulates the distribution between the locality of x and the broader graph structure.

The transport distance between two probability measures m_x^α and m_y^α, where $x, y \in V$, is defined as the first-order Wasserstein distance (Vaserstein, 1969; Anderes et al., 2016; Panaretos and Zemel, 2019):

$$W_1(m_x^\alpha, m_y^\alpha) = \inf_{\pi \in \Pi(m_x^\alpha, m_y^\alpha)} \sum_{u,v \in V} \pi(u, v) d(u, v), \tag{2}$$

where, $\pi(u, v)$ represents the probability mass transported from vertex u to vertex v, while $d(u, v)$ is the shortest path distance between u and v. The coupling measure $\pi(u, v)$ ensures that the total mass distribution is conserved and satisfies the conditions defined by the probability measures m_x^α and m_y^α. Finally, the Ollivier-Ricci curvature between two vertices x and y is defined as:

$$\kappa^\alpha(x, y) = 1 - \frac{W_1(m_x^\alpha, m_y^\alpha)}{d(x, y)}, \tag{3}$$

where W_1 refers to the first-order Wasserstein distance between the probability measures m_x^α and m_y^α. It is also commonly known as the Earth Mover's Distance, which quantifies the cost of transporting one probability distribution into another.

This formula quantifies the deviation of the graph from being a Euclidean metric space in terms of how the cost of optimal transport between probability distributions differs from the geometric distance between points.

The value of the hyperparameter α used in the calculation of Ollivier-Ricci curvature (using Eq. (3)) depends on the specific context and application. In the Ollivier-Ricci curvature framework, α typically represents a parameter that controls the sensitivity of the curvature calculation to the underlying geometric structure of the space being analyzed. The choice of α can influence the interpretation and behavior of the curvature measurements.

"Typically, α is a positive scalar value that can be adjusted based on the desired properties of the curvature analysis and the specific context in which the method is applied (Ollivier, 2009; Ni et al., 2019). Common choices for α include values such as 0.5, 1.0, or other numbers, depending on the extent to which one wishes to focus on local neighborhoods versus broader connections in the graph. In our analysis, we select $\alpha = 0.5$, a choice that balances local and global influences in order to provide a more well-rounded interpretation of the underlying structure."

In the computational analysis of network structures, the shortest path distances $d(u, v)$ between nodes are crucial for the calculation of the optimal transport distance (Wasserstein distance), which underpins the assessment of Ollivier-Ricci curvature. Two primary methodologies are employed for determining these shortest path distances:

- *All-Pairs Shortest Path (APSP)*: For comprehensive network analyses where repeated distance queries are expected, an all-pairs shortest path approach is utilized. This method leverages the efficient graph processing capabilities of NetworKit (Angriman et al., 2023; Staudt et al., 2016) to compute and store the shortest path distances between all node pairs in the graph. The resulting distance matrix, obtained using NetworKit's APSP function (Kuhn and Schneider, 2020; Vaid et al., 2017), provides a readily accessible source of shortest path data, facilitating efficient curvature calculations across the entire network.

- *Pairwise Shortest Path*: In scenarios where specific node pair distances are required, a pairwise approach is adopted. This method uses the Bidirectional Dijkstra algorithm (Rahayuda and Santiari, 2021; Vaira and Kurasova, 2011) from NetworKit to compute the shortest path between any given pair of source and target nodes directly. This targeted approach avoids the computational overhead of calculating and storing shortest paths for all node pairs, optimizing performance when only a subset of distances is needed.

3.2. Forman-Ricci curvature

In the study of simple network structures such as graphs, where only nodes and edges are present without more complex topological features, understanding curvature becomes more straightforward. In these settings, each edge directly connects two nodes without involving additional hierarchical relationships. This simplicity is advantageous when applying concepts of Ricci curvature, making it easier to analyze and visualize. Particularly, we explore the Forman-Ricci curvature, which is especially suited for analyzing networks that are structurally straightforward. The Forman-Ricci curvature adapts well to such basic topologies, providing valuable insights into the geometric properties of networks.

In this case, the Forman-Ricci curvature (Weber et al., 2017; Sreejith et al., 2016) is defined as:

$$\varsigma^{\alpha}(x, y) = \omega_\alpha \left[\frac{\omega_x}{\omega_\alpha} + \frac{\omega_y}{\omega_\alpha} - \sum_{\alpha_x, \alpha_y \sim \alpha} \left(\frac{\omega_x}{\sqrt{\omega_\alpha \omega_{\alpha_x}}} + \frac{\omega_y}{\sqrt{\omega_\alpha \omega_{\alpha_y}}} \right) \right], \tag{4}$$

where ω_α, ω_x, and ω_y denote the weights of the edge α, the nodes x and y, respectively. In addition, α_x and α_y denote the set of edges connecting x and y, respectively, but excluding the edge α.

Because we use unweighted network graphs in this study, we use a simplified mathematical formulation version of the Forman-Ricci curvature calculation (Forman, 2003; Sreejith et al., 2016), in which:

- Definition of Neighbors and Sets: we define α_x^0 and α_y^0 as the sets representing the neighbors of nodes α_x and α_y, respectively. These sets include both the predecessors and successors of α_x and α_y if the network is directed, or simply the neighbors of α_x and α_y if the network is undirected. Additionally, f is defined as the set containing the common neighbors between α_x^0 and α_y^0, i.e., the nodes that are neighbors of both. On the other hand, p is defined as the set containing the neighbors of α_x^0 or α_y^0 that are not common between them.

- Finally, the calculation of the Ricci-Forman Curvature for the Edge (α_x, α_y) is defined as $\mathcal{F}(\alpha_x, \alpha_y) = |f| + 2 - |p|$.

This concept of curvature is inherently linked to edges, making Forman curvature particularly well-suited for networks. Unlike other approaches, Forman curvature does not require any additional methods to extend curvature measurements from nodes to edges. However, although Forman curvature is primarily defined on edges (as a discretization of Ricci curvature), it can be gracefully extended to nodes as follows.

For each node n in the graph, the Ricci-Forman curvature is calculated as the average of curvatures of edges adjacent to node, i.e., $\sum_{(\alpha_x, \alpha_y) \text{ adjacent to } n} \mathcal{F}(\alpha_x, \alpha_y)/\deg(n)$.

3.3. Discrete Ricci Flow

Discrete Ricci flow (Ni et al., 2018, 2019) in graph theory is an innovative approach to iteratively adjust edge weights to achieve a uniform distribution of Ricci curvature across a network. This method is inspired by the continuous Ricci flow introduced by Richard S. Hamilton, which has significantly influenced geometric analysis by enabling the modification of a manifold's metric to evenly distribute curvature (Hamilton, 1982).

In the analysis of networks, we define discrete Ricci flow as a sequence of edge-weighted graphs $(V, E, \omega^{(\epsilon)})$, where $\epsilon \in \mathbb{Z}_{\geq 0}$ denotes discrete time steps (for this study $\epsilon = 50$). The weights of edges at each step are $\omega_{xy}^{(\epsilon)}$, and $d^{(\epsilon)}(x, y)$ is the shortest path length between vertices x and y under these weights. The evolution of edge weights is governed by the Ricci curvature $\kappa^{(\epsilon)}(x, y)$ at each edge xy as follows:

$$\omega_{xy}^{(\epsilon+1)} = (1 - \kappa^{(\epsilon)}(x, y))d^{(\epsilon)}(x, y), \tag{5}$$

where $\kappa^{(\epsilon)}(x, y)$ is calculated from the Ollivier-Ricci curvature, previously defined in Eq. (3).

For unweighted graphs $G = (V, E)$, the Ricci flow process begins with all initial edge weights $\omega_{xy}^{(0)}$ set to 1. This iterative application of the Ricci flow tends to contract subgraphs with positive Ricci curvature and expand those with negative curvature, mimicking the heat diffusion behavior observed in Riemannian manifolds. As the flow progresses, edges between different communities increase in weight, potentially approaching infinity, while those within communities decrease towards zero, thereby partitioning the network into distinct communities. This segmentation of the network is akin to the edge removal strategy employed in the Girvan-Newman algorithm, which is based on betweenness centrality (Girvan and Newman, 2002).

However, Ricci flow offers advantages over betweenness centrality as it does not require global information about the network and is computationally less intensive. It adjusts edge weights based solely on local curvature and adjacent node distances, providing a simpler and potentially more efficient mechanism for detecting and refining community structures in large networks, particularly those with hierarchical community structures.

3.4. Visibility Graph Analysis Algorithm

We have employed Visibility Graph Analysis (VGA) to transform the time series of CRs counts into complex networks. This process involves calculating the proximities and visibilities of each node in the series relative to all others. As a result, we obtain a complex network that preserves the topological and geometric information of the original time series.

The VGA algorithm (Lacasa and Toral, 2010; Stephen et al., 2015) operates by treating each data point in the time series as a node in the network. Connections between nodes are established based on a visibility criterion: a direct line of sight from one data point to another must not be obstructed by any intermediate data points. Specifically, two nodes a and b in the time series are connected if a straight line drawn from a to b does not intersect the vertical line extending from any intermediate data point. This transformation allows the intrinsic properties of the time series to be studied through the lens of network theory, analyzing aspects such as the network's topology and connectivity to uncover patterns and behaviors inherent in the original data.

VGA serves as a similarity algorithm by establishing the importance of each node in the series as a measure of its relationship with previous or subsequent nodes in terms of unobstructed distance. Although it is not strictly a similarity metric, the visibility criterion effectively captures the local and global structural relationships within the time series.

The algorithm can be described mathematically as follows. Consider a time series $\{x(t)\}_{t=1}^{N}$, where $x(t)$ represents the data value at time t. Each data point $x(t)$ is treated as a node in the visibility graph. Two nodes $x(t_i)$ and $x(t_j)$ are connected if they satisfy the following visibility criterion:

$$x(t_k) < x(t_i) + \frac{t_k - t_i}{t_j - t_i}(x(t_j) - x(t_i)) \quad \forall \quad t_i < t_k < t_j, \tag{6}$$

where t_i, t_j, and t_k are indices such that $t_i < t_j$ and $t_i < t_k < t_j$. This criterion ensures that the direct line of sight between $x(t_i)$ and $x(t_j)$ is not obstructed by any intermediate data point $x(t_k)$. By applying VGA, the algorithm convert the temporal information into a spatial network representation, allowing for a more comprehensive analysis of the time series through the interconnected relationships among nodes. This criterion ensures that a direct line of sight between $x(t_i)$ and $x(t_j)$ is not obstructed by any intermediate data point $x(t_k)$.

Next, we proceed to extract geometric and topological features from this network to analyze the structure and properties of the CRs count data. By applying VGA, we convert the temporal information into a spatial network representation, allowing for a more comprehensive analysis of the time series through the interconnected relationships among nodes.

3.5. Availability of Python Codes for Ricci Curvature Measurements

Despite the relative complexity and algorithmic intricacy of the aforementioned measures, several Python codes have already been developed to facilitate these tasks on discrete complex networks. In this work, we leverage a set of algorithms and libraries specifically designed for this purpose by Ni et al. (2019), which are readily accessible to all users. These tools are available for public use and can be found at the following web address: `https://github.com/saibalmars/GraphRicciCurvature`. In other words, for the VGA algorithm, I have developed a custom code based on a Python library that is publicly available at `https://pypi.org/project/ts2vg/`.

4. Results and discussions

We present both the distribution of time series counts and the complex network derived from these time series for several neutron monitors considered in this study in Figure 1. The counts are displayed for four stations located at high and mid-latitudes across both northern and southern hemispheres, illustrating the temporal variability in CRs counts at each location. Moreover, the complex network representation, constructed based on similarities in time series data, elucidates the interconnection structure among the neutron monitoring stations.

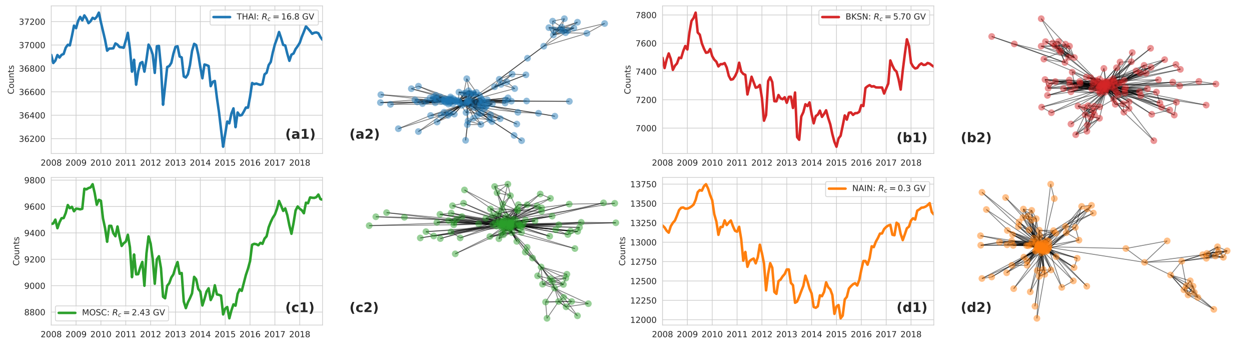

Figure 1: Distribution of the time series counts and the complex network generated from them. The plots on the left show the temporal evolution of cosmic ray counts for four neutron monitors at various latitudes (both northern and southern hemispheres). In the network plots on the right, each node represents a data point (or time step) from the corresponding time series, while edges denote a direct 'line of sight' or similarity relation among data points based on the visibility criterion. This network visualization highlights how the patterns in cosmic ray counts connect individual data points within each neutron monitoring station, offering insights into their proximity and mutual visibility as a function of recorded cosmic ray counts.

Figure 1 illustrates both the temporal variation of CRs counts at four representative neutron monitoring stations and the corresponding network representation derived from their time series. In the plots (a1), (b1), (c1), (d1), each station's count data are displayed over the same time interval, revealing distinct fluctuations associated with its geographic location and local geomagnetic conditions. On the plot (a2), (b2), (c2), (d2), a force-directed layout is used to position the stations as nodes, where edges reflect similarities or "visibilities" in their respective time series. Stations that share more closely correlated fluctuations are drawn closer together or exhibit denser connections, underscoring how patterns in CRs intensity may coincide across different latitudes or geomagnetic environments. By juxtaposing the raw time series with the network representation, the figure demonstrates that the construction of a complex network from the data captures non-linear hidden intrinsic relationships among stations. This approach provides an intuitive visualization of how variations in CRs counts lead to varying degrees of interconnectedness, with each edge indicating a significant temporal correspondence rather than mere geographic proximity.

The summary statistics for CRs intensity counts at the neutron monitor stations reveal several important insights shows in Table 2 for descriptive statistics about time series counts.

Table 2: Descriptive and network-based statistics for the time series data analyzed in this study. The columns in the table report the mean and standard deviation of the observations (MEAN, STD), the minimum and maximum values (MIN, MAX), skewness and kurtosis (SKEW, KURT), the entropy and fractal dimension correlation (ENTROPY, FRACTAL), and several graph-theoretical measures such as Average Degree Centrality (ADC), Average Clustering Coefficient (ACC), Average Path Length (APL), and Density.

No	Monitor	R_c	MEAN	STD	MIN	MAX	SKEW	KURT	ENTR	FRAC	ADC	ACC	APL	Dens
1	BRBG	0.01	9910.83	379.60	9206.59	10523.53	-0.14	-1.44	0.64	4.26	11.15	6.85	2.91	1.11
2	MRNY	0.03	7328.90	278.07	6723.56	7804.29	-0.21	-0.97	0.47	18.84	9.59	6.76	3.03	0.96
3	INVK	0.30	3582.81	128.27	3342.30	3789.45	-0.15	-1.30	0.50	-2.16	9.39	6.82	4.09	0.94
4	FSMT	0.30	6623.60	267.19	6106.27	7079.76	-0.05	-1.20	0.64	-0.16	9.54	7.00	2.98	0.95
5	THUL	0.30	123.68	4.63	115.20	131.91	-0.00	-1.28	0.72	3.87	8.96	6.97	3.16	0.90
6	NAIN	0.30	6566.66	232.76	6109.20	6989.02	-0.16	-1.18	0.56	-12.01	10.20	6.98	3.07	1.02
7	APTY	0.65	3953.06	151.24	3678.19	4198.45	-0.12	-1.26	0.58	-20.98	9.67	7.02	3.06	0.97
8	SNAE	0.73	168.12	6.65	155.32	179.91	-0.15	-1.10	0.60	-0.62	8.81	6.96	3.38	0.88
9	OULU	0.80	3279.69	116.36	3059.01	3481.06	-0.16	-1.23	0.60	14.49	10.31	6.93	3.20	1.03
10	KERG	1.14	225.68	8.02	210.30	237.90	-0.17	-1.34	0.53	-20.06	8.76	6.83	2.87	0.88
11	NEWK	2.40	1784.84	81.56	1633.04	1909.57	-0.16	-1.29	0.76	-0.59	8.91	7.25	3.50	0.89
12	MOSC	2.43	9298.18	285.48	8752.56	9769.25	-0.20	-1.30	0.65	-30.84	8.59	7.21	3.00	0.86
13	IRK2	3.64	5786.29	248.22	5319.07	6196.61	-0.26	-1.06	0.43	9.07	8.65	7.45	3.01	0.87
14	LMKS	3.84	1561.78	44.52	1457.79	1652.98	0.12	-0.54	0.87	-1.24	7.46	6.86	3.36	0.75
15	JUNG1	4.50	369.21	15.27	336.04	401.55	-0.07	-0.51	0.89	2.86	7.93	7.01	3.04	0.79
16	JUNG	4.50	160.66	4.85	149.41	169.00	-0.18	-0.98	0.63	1.35	7.67	6.65	4.08	0.77
17	HRMS	4.58	122.13	3.00	116.10	127.00	-0.22	-1.10	0.66	1.87	7.91	7.00	3.75	0.79
18	BKSN	5.60	7316.94	196.47	6867.91	7816.77	-0.05	-0.42	0.61	2.42	8.03	7.50	2.71	0.80
19	AATB	6.69	1405.67	35.12	1296.19	1452.20	-1.31	1.21	0.91	9.27	6.57	7.24	3.42	0.66
20	MXCO	8.20	13637.55	216.36	13112.05	13990.88	-0.22	-0.84	0.93	-2.99	7.82	7.37	2.99	0.78
21	TSMB	9.29	330.26	5.07	317.41	339.90	-0.06	-0.62	0.52	-9.56	7.23	7.32	3.08	0.72
22	PSNM	16.80	18743.96	124.60	18366.52	18948.99	-0.81	0.27	0.98	14.72	6.89	7.30	3.38	0.69

From the data in Table 2, it is evident that neutron monitoring stations located in regions with higher R_c tend to exhibit greater kurtosis and reduced skewness in their time series, whereas stations at lower rigidity display more pronounced skewness coupled with lower kurtosis (and often negative) values (Takalo, 2022; Sierra-Porta, 2024; Koeksal et al., 2021). One possible explanation for this pattern lies in the varying degrees of geomagnetic filtering: higher-rigidity stations may experience occasional surges or sharp peaks in CRs counts—raising the likelihood of more pronounced, short-duration extrema—thus increasing kurtosis and reducing overall asymmetry in the distribution. In contrast, stations subject to lower rigidity likely record a broader range of moderate fluctuations, producing flatter distributions with heavier tails shifted in one direction (more negative skewness), as the reduced geomagnetic shielding allows for smoother but more diverse variations in detected CRs. These contrasting profiles highlight the impact of local geomagnetic conditions on the statistical properties of CRs time series, suggesting that the interplay between R_c and the underlying CRs flux dynamics leads to distinctly different distributional shapes across neutron monitoring stations.

Aditionally, from direct inspection on Table 2, it is possible to discern that stations at higher R_c generally exhibit higher entropy in their CRs time series, suggesting a wider or more disordered range of fluctuations. This tendency is particularly noticeable in stations with $R_c \geq 5$ GV, which cluster toward entropy values exceeding 0.8 and, in some cases, approach 1.0. By contrast, stations with lower rigidity (e.g., below 1.0–2.0 GV) display moderate to lower entropy, indicating a less varied distribution of CRs counts. The entropy and fractal dimension measures also offer valuable information about the complexity and irregularity of the time series. Stations with higher entropy values, such as MXCO and PSNM, indicate greater unpredictability and complexity in CRs counts. On the other hand, stations with lower entropy values, such as INVK, FSMT and MRNY, suggest more regular and predictable patterns.

In other words, depicting fractal dimension correlation, the values span a broader range—some stations with low rigidity can exhibit both positive and negative extremes—while higher-rigidity stations tend to cluster at more negative values. Although no strict linear relationship is immediately apparent, the overall pattern suggests that as rigidity increases, the CRs series may assume a more "peaked" or sharply fluctuating structure (captured by higher entropy), but also exhibit lower fractal dimension correlation. These dual tendencies imply that geomagnetic conditions not only influence the breadth of variability in CRs fluxes, as reflected by entropy, but may also dampen long-range correlations or scaling behaviors, leading to a decrease in fractal-like complexity in regions of elevated geomagnetic cut-off rigidity.

Additionally to statistical properties of CRs time series, we quantitatively assess the network structure of neutron monitoring stations by analyzing graph centrality measures (see Figure 2). These measures include: degree centrality

(ADC), betweenness centrality (ABC), closeness centrality (ACC), eigenvector centrality (EC), clustering coefficient (CC), diameter (Dia), average path length (APL), assortativity (AC) and density (Den).

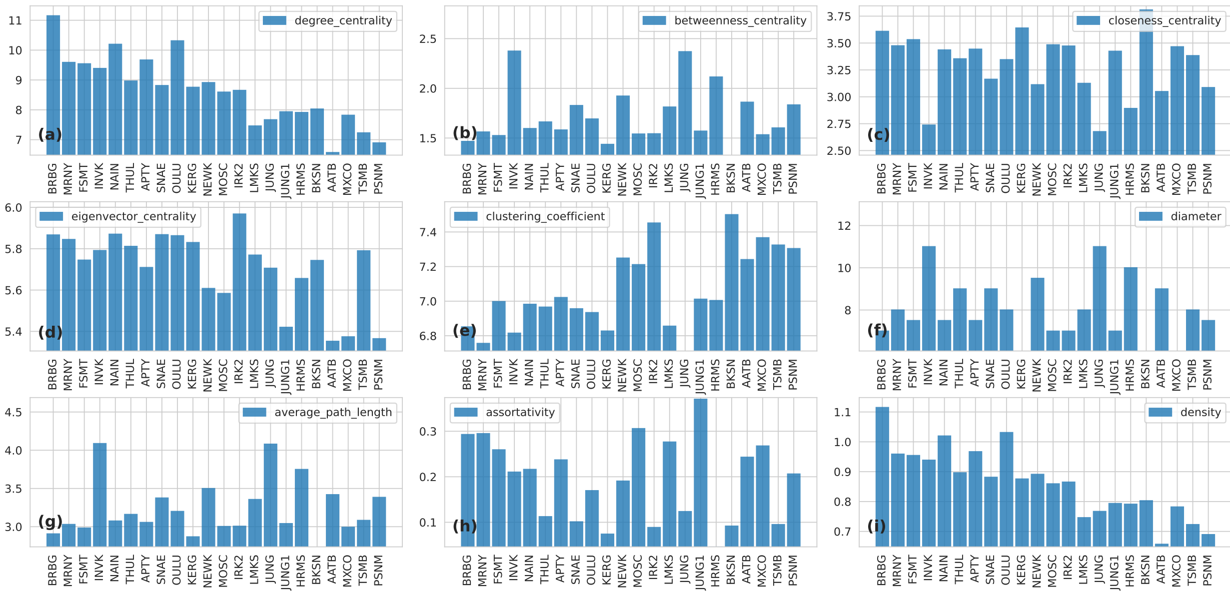

Figure 2: Graph centrality measures across neutron monitoring stations, arranged from lowest to highest R_c. The figure illustrates average degree centrality, average betweenness centrality, assortativity, and mean degree distribution, revealing patterns of connectivity and network structure influenced by geomagnetic cutoff rigidity effects.

In terms of network measures derived from the visibility graph and network analysis, the ADC, ACC, EC, and Denity provide insights into the structural properties of the networks.

Actually, the ADC (Fig. 2(a) indicates the immediate connectivity of a node within the network. We observed higher ADC values at stations with lower cutoff rigidities, generally located at higher latitudes. This suggests denser connectivity at these sites, potentially due to the lower R_c against CRs, which allows for more extensive and frequent CRs interactions. In contrast, stations positioned at higher latitudes, which experience lower R_c, exhibit lower average degree centrality, reflecting a sparser connectivity pattern. This pattern aligns with the protective effect of Earth's magnetic field, which intensifies with latitude and influences CRs penetration. Higher ADC values, as seen in BRBG, MNRY and FSMT, indicate a more interconnected network, suggesting that these stations have more similar patterns of CRs counts with other stations but also coincide with stations a lower R_c. Conversely, stations with high R_c have more dispersed and less interconnected nodes (e.g. AATB, TSMB and PSNM).

In other words, high ACC values (see Fig. 2(e)), such as those observed in MXCO, TSMB, and PSNM, indicate a strong tendency for stations to form tightly knit clusters within the network. The ACC is a measure of the degree to which nodes in a network tend to cluster together, capturing the local interconnectedness of the network. This suggests that these stations, characterized by higher ACC values, may share similar geographical or geomagnetic influences and are associated with higher magnetic rigidity (R_c). These tightly connected clusters could reflect underlying relationships in cosmic ray dynamics and their interactions with geomagnetic and atmospheric conditions.

The density metric (Fig- 2(i)) reveals a clear relationship with the R_c. Stations with lower rigidity cutoff values exhibit significantly higher density values, such as BRBG and MRNY, which both show densely interconnected networks. This suggests that cosmic ray time series at these stations are characterized by more consistent temporal correlations, likely influenced by strong geomagnetic shielding effects. As R_c increases, the density decreases, as observed in stations like PSNM, TSMB and MXCO. This trend indicates sparser network structures, reflecting the impact of broader heliospheric effects and the less localized temporal consistency of cosmic ray intensities at these stations.

This relationship between R_c and density highlights how geomagnetic and heliospheric conditions influence the interconnectivity of the underlying network structure, making density a valuable metric for understanding cosmic ray variability across different stations.

Based on the graph showing EC (Fig. 2(d)) values across neutron monitoring stations ordered by increasing magnetic rigidity (R_c), the following observations can be made. Eigenvector centrality, a measure that reflects the influence of a node in a network based not only on its direct connections but also on the importance of the nodes it is connected to, exhibits a subtle pattern across the stations. Stations with lower magnetic rigidity (e.g., BRBG, MRNY, INVK, FSMT) display relatively higher eigenvector centrality values, suggesting these stations play a more central and influential role in the network structure. This centrality might be indicative of their prominence in facilitating connections between other highly connected stations, potentially driven by their geomagnetic and geographical characteristics.

As geomagnetic rigidity increases, eigenvector centrality shows a decreasing trend, with stations like MXCO, TSMB, and PSNM exhibiting the lowest values. This pattern indicates that stations with higher R_c tend to be less influential in the network's broader structure. This could result from their peripheral positions in terms of the cosmic ray dynamics represented in the network, where their local interactions might dominate over their global influence.

This analysis suggests a general inverse relationship between eigenvector centrality and magnetic rigidity, highlighting how the structural importance of stations diminishes as R_c increases. This trend may reflect the changing dynamics of cosmic ray propagation and geomagnetic shielding across different latitudes and rigidities.

Additionally, the AC, which evaluates the likelihood of nodes connecting with others that have similar or dissimilar degrees, show varying assortativity across the network, which helps in understanding the clustering behavior and the propensity of nodes to form tightly knit groups (see Fig. 2(h)). Although there is no clear trend regarding its variation with respect to latitude, it differs significantly with respect to the monitor stations, with different behaviors in different CRs counting monitors.

Moreover, the ABC and ACC (Fig. 2(b) and 2(c), respectively) provides insights into the role of specific nodes in facilitating communication across the network. No clear trend is evident. APL and Diameter (Fig. 2(g) and 2(f), respectively), no clear relationship with R_c is evident from the data.

The results of the calculation of Ollivier-Ricci, Forman-Ricci, and Ricci Flow metrics for all neutron monitoring stations worldwide are presented graphically in Figure 4, showing a bar chart. On the x-axis, the neutron stations are ordered from lowest to highest R_c, from left to right. In this representation, the mean value of each of the curvature measurements for all stations is observed.

In the analysis of the neutron monitor stations network, the Ricci flow, along with Olivier-Ricci and Forman-Ricci curvatures, serve as discrete local measures for each node. To synthesize these individual metrics into a broader perspective of the network's dynamics, we aggregated these local values through the construction of a histogram encompassing measures for all nodes. This method averages the local measures, yielding a global representation that effectively captures the overall behavior of the network.

The Figure 3 shows the variation in Olivier-Ricci curvature, Forman-Ricci curvature, and Ricci flow across a range of CRs monitor stations ordered by increasing latitude. Analyzing these metrics provides insights into the topological robustness and connectivity differences among these stations.

The upper panel in Figure 3, displaying the Olivier-Ricci curvature, shows slight variations across the latitude. Olivier-Ricci curvature, which typically reflects the edge-based connectivity relative to the network's average connectivity, appears to have minor fluctuations that could indicate a relatively uniform network structure with few anomalies in connectivity or network density. However, no clear correlation is observed between this Olivier-Ricci curvature value and the R_c of the stations, as evidenced by a poor correlation coefficient of 0.28.

The middle panel in Figure 3 illustrates the Forman-Ricci curvature, which evaluates edge curvature by taking into account node and edge weights. Lower values of this measure often suggest stronger and more robust connections. As can be seen, there seems to be a tendency for the time series of neutron monitor stations at small latitudes to have stronger connections, possibly indicating regions with dense interconnections or a significant group of stations with these characteristics.

Additionally, we observe a slight correlation indicating that as R_c increases, the Forman-Ricci curvature tends to rise modestly. Specifically, we calculate a moderate to high correlation coefficient of -0.86 demonstrating an inverse relationship between R_c and Forman-Ricci curvature. This finding suggests that stations with higher R_c might exhibit more complex or tightly interconnected network structures as measured by the Forman-Ricci curvature.

The lower panel in Figure 3 depicts Ricci flow values, which are derived from iteratively applying Ricci curvature adjustments to refine the network's topology. This analysis suggests a correlation between the station's latitude and variations in network topology as measured by these Ricci curvatures (correlation coefficient of -0.92). Specifically, it

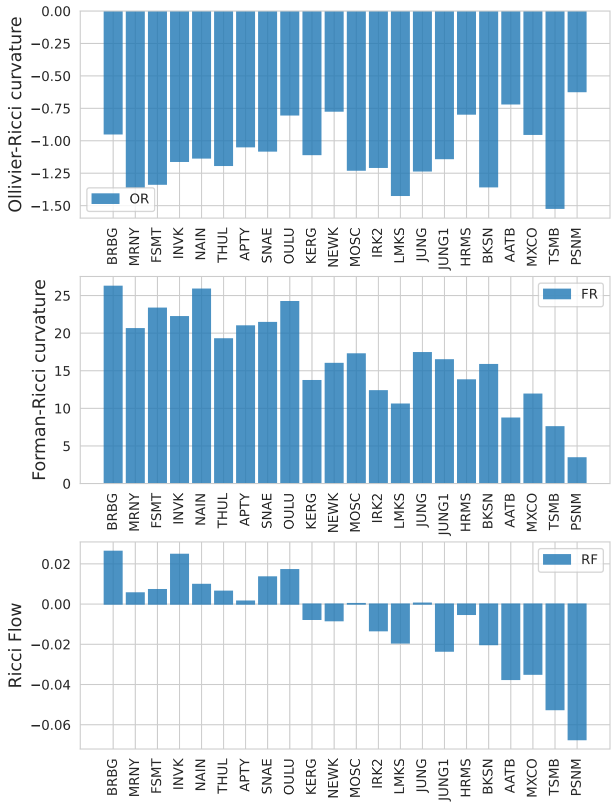

Figure 3: Bar charts illustrating the OR, FR and RF metrics for neutron monitoring stations. The stations are ordered along the x-axis, and their corresponding curvature metrics are displayed on the y-axis. The OR metric shows generally negative values across stations, with some variability. The FR metric demonstrates a clear decreasing trend as magnetic rigidity increases from left to right, reflecting its inverse relationship with geomagnetic rigidity. Similarly, the RF metric exhibits predominantly negative values that decrease further for stations with higher magnetic rigidity, consistent with the trends observed in our analysis. These patterns emphasize the geometric properties captured by the curvature metrics in relation to cosmic ray dynamics.

appears that stations at certain latitudes might share more similar network characteristics, possibly due to similar environmental influences or operational factors affecting CRs detection. Stations in closely situated latitudes might show similar topological robustness and network integration, possibly reflecting regional clustering in how CRs phenomena are monitored and analyzed. This analysis provides a quantifiable insight into how the physical and operational characteristics of stations influence the overall network dynamics and detection capabilities.

In network analysis, “Average Ricci flow” is understood as the mean value of Ricci flow metrics applied across all edges of a network over a specified period or throughout different regions of the network. This statistical measure offers insights into the network’s structural evolution, reflecting how Ricci flow influences the network’s topology over time.

Networks characterized by small Ricci flow values typically exhibit uniform or minimally varying curvature across their edges. Observations from neutron monitor stations at lower latitudes indicate that these stations tend to exhibit smaller Ricci flow values, pointing to a more stable and uniform network behavior in these regions. Conversely, networks with large Ricci flow values indicate significant variations in curvature across edges, signaling ongoing substantial adjustments in the network’s structure.

Inspired by the previous finding of significant correlations, particularly regarding the Forman-Ricci and Ricci Flow metrics, we further explore the complex networks of each neutron monitor station. We now develop and calculate simple models to establish an explicit and mathematically established relationship R_c and curvature.

For the Forman-Ricci metric, a model that fits well consists of $R_c = a_1 + b_1 \exp(-c_1 \mathrm{FR})$, where FR is the Forman-Ricci metric, and $a_1 = -0.663 \pm 0.843$, $b_1 = 26.257 \pm 2.340$, and $c_1 = 0.128 \pm 0.020$. This model achieves a Root Mean

Square Error (RMSE) of 0.31 and an r^2-score (coefficient of determination) of 0.86, indicating both high predictive accuracy and strong explanatory power regarding the observed variability in cosmic ray intensities at the neutron monitoring stations under consideration (see Fig. 3(middle panel)).

However, when establishing the relationship between the R_c of neutron monitoring stations and the Ricci Flow, the results indicate a good fit of the form $R_c = a_2 + b_2 \exp(-c_2 \mathrm{RF})$, where RF is the Ricci flow metric, and $a_2 = -2.866 \pm 1.400$, $b_2 = 4.732 \pm 1.391$, and $c_2 = 20.577 \pm 3.609$. This model yields an RMSE of 0.24 and an r2-score of 0.92. The results are shown graphically in Figure 3(lower panel). This result is consistent and in line with previous results using different methodologies from the studies of Sierra-Porta and Domínguez-Monterroza (2022); Sierra-Porta (2024).

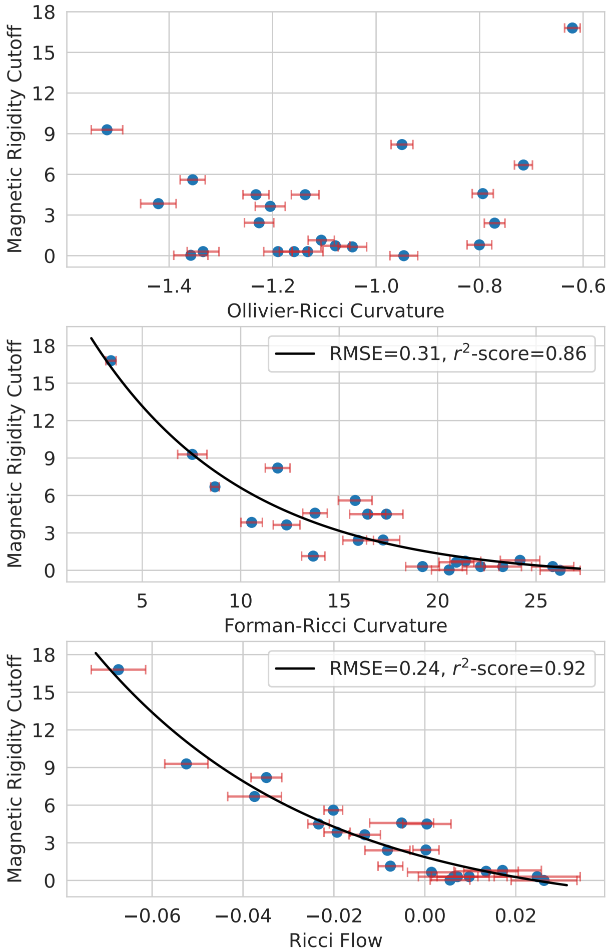

Figure 4: Scatter plot showing the relationship between curvature metrics (Forman-Ricci and Ricci Flow) and geomagnetic cutoff rigidity of neutron monitoring stations. Mathematical fit relationships are included for each metric, highlighting the trend observed in the data and the quality of the model fit.

To assess statistical significance of the correlations between the curvature metrics OR, FR, RF and the R_c, Pearson's correlation, Spearman's rank correlation, and Kendall's tau tests at a significance level of $\alpha = 0.05$ (95% confidence) has perform. For Ollivier-Ricci curvature, the Pearson test yielded $r = 0.2809$ with $p = 0.2055$, Spearman's rank correlation showed $\rho = 0.1167$ with $p = 0.6051$, and Kendall's tau yielded $\tau = 0.0879$ with $p = 0.5713$. All of these p-values are greater than 0.05, indicating that there is no statistically significant correlation between OR and R_c.

In contrast, for Forman-Ricci curvature, the Pearson test gave $r = -0.8524$ with $p = 4.76 \times 10^{-7}$, the Spearman test showed $\rho = -0.8570$ with $p = 3.53 \times 10^{-7}$, and Kendall's tau gave $\tau = -0.6770$ with $p = 1.30 \times 10^{-5}$. These extremely small p-values provide strong evidence of a highly significant negative correlation between FR and R_c. Similarly, for Ricci Flow, the Pearson test resulted in $r = -0.9204$ with $p = 1.32 \times 10^{-9}$, the Spearman test showed $\rho = -0.8876$ with $p = 3.63 \times 10^{-8}$, and Kendall's tau gave $\tau = -0.7298$ with $p = 2.62 \times 10^{-6}$. These results also indicate a very strong and statistically significant negative correlation between RF and R_c.

In summary, at the 95% confidence level, Forman-Ricci curvature and Ricci Flow display robust and highly significant negative correlations.

5. Conclusions

In this research we have applied an innovative RC count time series analysis using advanced topological techniques by introducing the construction of complex networks using VGA and network geometry. This approach has allowed us to systematically capture interactions between neutron detectors distributed around the world, thus providing a structured and understandable representation of the global CR monitoring network.

By calculating explicit curvature metrics for each generated complex network, we have unearthed two fundamental findings. First, we have observed a remarkable and direct correlation between the Forman-Ricci metric and the geomagnetic cutoff rigidity of the neutron detectors. This association, characterized by a proportional relationship, sheds light on the influence of magnetic stiffness on the topology and curvature of the neutron monitoring network.

On the other hand, we have found that the Ricci Flow exhibits an inverse relationship with the magnetic stiffness of the neutron detectors. This association suggests an interesting dynamic in which detectors with higher rigidity tend to have lower Ricci Flow, while those with lower rigidity experience higher Ricci Flow. This observation provides valuable insight into the variability and complexity of CRs count time series at different latitudes and geographic locations.

These results underscore the importance of considering network topology and curvature metrics in the analysis of CRs count time series. Curvature metrics, especially Forman-Ricci and Ricci Flow, emerge as powerful tools to characterize the dynamics of complex neutron monitoring networks and to unravel hidden patterns and underlying relationships in the data.

In conclusion, our study not only advances the understanding of the complex dynamics of CRs counts, but also opens new perspectives for improving space weather prediction by including features derived from network topology and curvature metrics in more advanced and robust predictive models. This integrative approach promises to provide a more complete and accurate understanding of space weather phenomena, which has important implications for mitigating risks associated with outer space conditions on Earth.

6. Final comments

As a final comment, it should be noted that this study marks the beginning of a deeper and more detailed exploration of the dynamics of CRs counts and their relationship to space weather. While we have obtained promising results in analyzing complex networks and associated curvature metrics, we recognize that much remains to be discovered.

A natural next step would be to incorporate data at higher temporal resolutions, such as hourly resolutions, to capture more complex elements and rarer, more distinctive phenomena in cosmic radiation. However, this brings with it the challenge of handling much longer time series, requiring greater computational power and additional resources.

In addition, the study could be enriched by introducing new variables associated with space weather, which would allow a more complete and accurate understanding of the relationships and patterns observed in the models.

Finally, an interesting approach that we have initiated is the use of Ricci Flow to detect communities and phenomena in the time series. From the results obtained in this study, we believe that Ricci Flow could be a powerful tool to identify outlier events and associate them with other space weather phenomena and variables. This approach promises to open new perspectives for the detection and understanding of rare and potentially important phenomena in cosmic radiation dynamics and space weather.

Acknowledgments

D.S.P. wishes to express sincere gratitude to the Research Office of the Universidad Tecnológica de Bolívar for its unwavering support and commitment during the development of this study. Although the research did not receive funding from any institution or entity, the author is thankful to the Directorate of UTB for providing computational equipment essential for the development of the algorithms, codes and results. The support provided has been fundamental in advancing our research processes and contributing to the knowledge in the field of space weather and cosmic radiation dynamics.

Data Availability Statement

While the data and codes used for algorithm development are freely accessible and have been identified in the paper, the complete dataset is available upon request.

References

P. K. Grieder, Cosmic rays at Earth, Elsevier, 2001. doi:https://ui.adsabs.harvard.edu/link_gateway/2001cre..book.....G/doi:10.1016/B978-0-444-50710-5.X5000-3.

J. F. Ziegler, Terrestrial cosmic rays, IBM journal of research and development 40 (1996) 19–39. doi:https://doi.org/10.1147/rd.401.0019.

V. Tatischeff, J. C. Raymond, J. Duprat, S. Gabici, S. Recchia, The origin of galactic cosmic rays as revealed by their composition, Monthly Notices of the Royal Astronomical Society 508 (2021) 1321–1345. doi:https://doi.org/10.1093/mnras/stab2533.

L. I. Dorman, Space weather and cosmic ray effects, in: Climate change, Elsevier, 2021, pp. 711–768. doi:https://doi.org/10.1016/B978-0-12-821575-3.00033-5.

M. Guhathakurta, Everyday space weather, Journal of Space Weather and Space Climate 11 (2021) 36. doi:https://doi.org/10.1051/swsc/2021019.

L. C. Simonsen, T. C. Slaba, P. Guida, A. Rusek, Nasa's first ground-based galactic cosmic ray simulator: Enabling a new era in space radiobiology research, PLoS biology 18 (2020) e3000669. doi:https://doi.org/10.1371/journal.pbio.3000669.

S. K. Höeffgen, S. Metzger, M. Steffens, Investigating the effects of cosmic rays on space electronics, Frontiers in Physics 8 (2020) 318. doi:https://doi.org/10.3389/fphy.2020.00318.

H. Köksal, N. Demir, A. Kilcik, Analysis of the cosmic ray effects on sentinel-1 sar satellite data, Aerospace 8 (2021) 62. doi:https://doi.org/10.3390/aerospace8030062.

A. B. Sharma, O. Lamba, A review: source and effect of mobile communication radiation on human health, Advances in Wireless and Mobile Communications 10 (2017) 423–435. doi:https://www.ripublication.com/awmc17/awmcv10n3_03.pdf.

A. Singh, D. Siingh, R. Singh, Impact of galactic cosmic rays on earth's atmosphere and human health, Atmospheric Environment 45 (2011) 3806–3818. doi:https://doi.org/10.1016/j.atmosenv.2011.04.027.

M. Lim, Cosmic rays: are air crew at risk?, Occupational and environmental medicine 59 (2002) 428–432. doi:https://oem.bmj.com/content/oemed/59/7/428.full.pdf.

F. A. Cucinotta, M. Durante, Cancer risk from exposure to galactic cosmic rays: implications for space exploration by human beings, The lancet oncology 7 (2006) 431–435. doi:https://doi.org/10.1016/S1470-2045(06)70695-7.

D. Sierra-Porta, On the fractal properties of cosmic rays and sun dynamics cross-correlations, Astrophysics and Space Science 367 (2022) 116. doi:https://doi.org/10.1007/s10509-022-04151-5.

W.-X. Zhou, Multifractal detrended cross-correlation analysis for two nonstationary signals, Physical Review E 77 (2008) 066211. doi:https://doi.org/10.1103/PhysRevE.77.066211.

K. Kudela, D. Venkatesan, Fractal structure of cosmic ray intensity variations, Nuclear Physics B-Proceedings Supplements 39 (1995) 127–135. doi:https://doi.org/10.1016/0920-5632(95)00015-2.

S. Gopinath, P. Prince, Multifractal characteristics of magnetospheric dynamics and their relationship with sunspot cycle, Advances in Space Research 59 (2017) 2265–2278. doi:https://doi.org/10.1016/j.asr.2017.02.011.

K. Herbst, A. Kopp, B. Heber, Influence of the terrestrial magnetic field geometry on the cutoff rigidity of cosmic ray particles, in: Annales Geophysicae, volume 31, Copernicus Publications Göttingen, Germany, 2013, pp. 1637–1643. doi:https://doi.org/10.5194/angeo-31-1637-2013.

D. Smart, M. Shea, A review of geomagnetic cutoff rigidities for earth-orbiting spacecraft, Advances in Space Research 36 (2005) 2012–2020. doi:https://doi.org/10.1016/j.asr.2004.09.015.

O. Danilova, N. Ptitsyna, M. Tyasto, V. Sdobnov, The relationship of magnetospheric parameters with cosmic-ray cutoff rigidities depending on latitude, Cosmic Research 61 (2023) 18–26. doi:https://doi.org/10.1134/S0010952523010021.

E. S. Comedi, A. G. Elias, B. S. Zossi, Spatial features of geomagnetic cutoff rigidity secular variation using analytical approaches, Journal of Atmospheric and Solar-Terrestrial Physics 211 (2020) 105475. doi:https://doi.org/10.1016/j.jastp.2020.105475.

M. Gerontidou, N. Katzourakis, H. Mavromichalaki, V. Yanke, E. Eroshenko, World grid of cosmic ray vertical cut-off rigidity for the last decade, Advances in Space Research 67 (2021) 2231–2240. doi:https://doi.org/10.1016/j.asr.2021.01.011.

D. Sierra-Porta, A.-R. Domínguez-Monterroza, Linking cosmic ray intensities to cutoff rigidity through multifractal detrented fluctuation analysis, Physica A: Statistical Mechanics and its Applications 607 (2022) 128159. doi:https://doi.org/10.1016/j.physa.2022.128159.

J. W. Kantelhardt, S. A. Zschiegner, E. Koscielny-Bunde, S. Havlin, A. Bunde, H. E. Stanley, Multifractal detrended fluctuation analysis of nonstationary time series, Physica A: Statistical Mechanics and its Applications 316 (2002) 87–114. doi:https://doi.org/10.1016/S0378-4371(02)01383-3.

A. Giri, B. Adhikari, S. Dahal, K. Paula, M. Bolzan, Multi-fractal analysis of cosmic rays over mid-and high-latitude stations during severe geomagnetic storms, Solar Physics 299 (2024) 148. doi:https://doi.org/10.1007/s11207-024-02393-w.

Z.-G. Yu, V. Anh, R. Eastes, Multifractal analysis of geomagnetic storm and solar flare indices and their class dependence, Journal of Geophysical Research: Space Physics 114 (2009). doi:https://doi.org/10.1029/2008JA013854.

D. Sierra-Porta, Relationship between magnetic rigidity cutoff and chaotic behavior in cosmic ray time series using visibility graph and network analysis techniques, Chaos: An Interdisciplinary Journal of Nonlinear Science 34 (2024). doi:https://doi.org/10.1063/5.0167156.

M. Stephen, C. Gu, H. Yang, Visibility graph based time series analysis, PloS one 10 (2015) e0143015. doi:https://doi.org/10.1371/journal.pone.0143015.

L. Lacasa, R. Toral, Description of stochastic and chaotic series using visibility graphs, Physical Review E 82 (2010) 036120. doi:https://doi.org/10.1103/PhysRevE.82.036120.

D. Sierra-Porta, A multifractal approach to understanding forbush decrease events: Correlations with geomagnetic storms and space weather phenomena, Chaos, Solitons & Fractals 185 (2024) 115089. doi:https://doi.org/10.1016/j.chaos.2024.115089.

M. Boguna, I. Bonamassa, M. De Domenico, S. Havlin, D. Krioukov, M. Á. Serrano, Network geometry, Nature Reviews Physics 3 (2021) 114–135. doi:https://doi.org/10.1038/s42254-020-00264-4.

D. Mulder, G. Bianconi, Network geometry and complexity, Journal of Statistical Physics 173 (2018) 783–805. doi:https://doi.org/10.1007/s10955-018-2115-9.

G. Salanti, F. K. Kavvoura, J. P. Ioannidis, Exploring the geometry of treatment networks, Annals of internal medicine 148 (2008) 544–553. doi:https://doi.org/10.7326/0003-4819-148-7-200804010-00011.

A. Samal, H. K. Pharasi, S. J. Ramaia, H. Kannan, E. Saucan, J. Jost, A. Chakraborti, Network geometry and market instability, Royal Society open science 8 (2021) 201734. doi:https://doi.org/10.1098/rsos.201734.

P. T.-W. Yen, K. Xia, S. A. Cheong, Understanding changes in the topology and geometry of financial market correlations during a market crash, Entropy 23 (2021) 1211. doi:https://doi.org/10.3390/e23091211.

M. Haenggi, Stochastic geometry for wireless networks, Cambridge University Press, 2012. URL: https://dl.acm.org/doi/abs/10.5555/2480878.

D. B. de Souza, J. T. Da Cunha, E. F. dos Santos, J. B. Correia, H. P. da Silva, J. L. de Lima Filho, J. Albuquerque, F. A. Santos, Using discrete ricci curvatures to infer covid-19 epidemic network fragility and systemic risk, Journal of Statistical Mechanics: Theory and Experiment 2021 (2021) 053501. doi:https://doi.org/10.1088/1742-5468/abed4e.

R. Albert, B. DasGupta, N. Mobasheri, Topological implications of negative curvature for biological and social networks, Physical Review E 89 (2014) 032811. doi:https://doi.org/10.1103/PhysRevE.89.032811.

G. Marti, F. Nielsen, M. Bińkowski, P. Donnat, A review of two decades of correlations, hierarchies, networks and clustering in financial markets, Progress in information geometry: Theory and applications (2021) 245–274. doi:https://doi.org/10.1007/978-3-030-65459-7_10.

O. M. Granados, A. Vargas, The geometry of suspicious money laundering activities in financial networks, EPJ Data Science 11 (2022) 6. doi:https://doi.org/10.1140/epjds/s13688-022-00318-w.

R. V. Donner, J. Heitzig, J. F. Donges, Y. Zou, N. Marwan, J. Kurths, The geometry of chaotic dynamics—a complex network perspective, The European Physical Journal B 84 (2011) 653–672. doi:https://doi.org/10.1140/epjb/e2011-10899-1.

A. Baptista, B. D. MacArthur, C. R. Banerji, Charting cellular differentiation trajectories with ricci flow, bioRxiv (2023) 2023–07. doi:https://doi.org/10.1101/2023.07.20.549833.

W.-L. Jin, Stability and bifurcation in network traffic flow: A poincaré map approach, Transportation Research Part B: Methodological 57 (2013) 191–208. doi:https://doi.org/10.1016/j.trb.2013.08.013.

M. Golubitsky, I. Stewart, Recent advances in symmetric and network dynamics, Chaos: An Interdisciplinary Journal of Nonlinear Science 25 (2015). doi:https://doi.org/10.1063/1.4918595.

R. A. El-Nabulsi, Fractal diffusion from a geometric ricci flow, Journal of Elliptic and Parabolic Equations 8 (2022) 837–852. doi:https://doi.org/10.1007/s41808-022-00169-6.

S. Gaidash, A. Belov, M. Abunina, A. Abunin, Space weather forecasting at izmiran, Geomagnetism and Aeronomy 57 (2017) 869–876. doi:https://doi.org/10.1134/S0016793217070088.

H. Mavromichalaki, A. Papaioannou, C. Sarlanis, G. Souvatzoglou, M. Gerontidou, C. Plainaki, M. Papailiou, G. Mariatos, N. Team, Establishing and using the real-time neutron monitor database (nmdb), in: 9th International Conference of the Hellenic Astronomical Society, volume 424, 2010, p. 75. doi:https://adsabs.harvard.edu/full/2010ASPC..424...75M.

H. Mavromichalaki, A. Papaioannou, C. Plainaki, C. Sarlanis, G. Souvatzoglou, M. Gerontidou, M. Papailiou, E. Eroshenko, A. Belov, V. Yanke, et al., Applications and usage of the real-time neutron monitor database, Advances in Space Research 47 (2011) 2210–2222. doi:https://doi.org/10.1016/j.asr.2010.02.019.

M. Weber, E. Saucan, J. Jost, Characterizing complex networks with forman-ricci curvature and associated geometric flows, Journal of Complex Networks 5 (2017) 527–550. doi:https://doi.org/10.1093/comnet/cnw030.

A. Tannenbaum, C. Sander, L. Zhu, R. Sandhu, I. Kolesov, E. Reznik, Y. Senbabaoglu, T. Georgiou, Graph curvature and the robustness of cancer networks, arXiv preprint arXiv:1502.04512 (2015). doi:https://doi.org/10.48550/arXiv.1502.04512.

M. Weber, J. Stelzer, E. Saucan, A. Naitsat, G. Lohmann, J. Jost, Curvature-based methods for brain network analysis, arXiv preprint arXiv:1707.00180 (2017). doi:https://doi.org/10.48550/arXiv.1707.00180.

R. Sandhu, T. Georgiou, E. Reznik, L. Zhu, I. Kolesov, Y. Senbabaoglu, A. Tannenbaum, Graph curvature for differentiating cancer networks, Scientific reports 5 (2015) 12323. doi:https://doi.org/10.1038/srep12323.

W. Leal, G. Restrepo, P. F. Stadler, J. Jost, Forman–ricci curvature for hypergraphs, Advances in Complex Systems 24 (2021) 2150003. doi:https://doi.org/10.1142/S021952592150003X.

R. S. Sandhu, T. T. Georgiou, A. R. Tannenbaum, Ricci curvature: An economic indicator for market fragility and systemic risk, Science advances

2 (2016) e1501495. doi:https://doi.org/10.1126/sciadv.1501495.
J. Topping, F. Di Giovanni, B. P. Chamberlain, X. Dong, M. M. Bronstein, Understanding over-squashing and bottlenecks on graphs via curvature, arXiv preprint arXiv:2111.14522 (2021). doi:https://doi.org/10.48550/arXiv.2111.14522.
K. Nguyen, N. M. Hieu, V. D. Nguyen, N. Ho, S. Osher, T. M. Nguyen, Revisiting over-smoothing and over-squashing using ollivier-ricci curvature, in: International Conference on Machine Learning, PMLR, 2023, pp. 25956–25979. doi:https://doi.org/10.48550/arXiv.2211.15779.
M. Weber, Neighborhood growth determines geometric priors for relational representation learning, in: International Conference on Artificial Intelligence and Statistics, PMLR, 2020, pp. 266–276. doi:https://doi.org/10.48550/arXiv.1910.05565.
Y. Ollivier, Ricci curvature of markov chains on metric spaces, Journal of Functional Analysis 256 (2009) 810–864. doi:https://doi.org/10.1016/j.jfa.2008.11.001.
Y. Ollivier, Ricci curvature of metric spaces, Comptes Rendus Mathematique 345 (2007) 643–646. doi:https://doi.org/10.1016/j.crma.2007.10.041.
L. N. Vaserstein, Markov processes over denumerable products of spaces, describing large systems of automata, Problemy Peredachi Informatsii 5 (1969) 64–72. doi:https://www.mathnet.ru/links/b5f77cc07d259e4f1788e16d6800dd72/ppi1811.pdf.
E. Anderes, S. Borgwardt, J. Miller, Discrete wasserstein barycenters: Optimal transport for discrete data, Mathematical Methods of Operations Research 84 (2016) 389–409. doi:https://doi.org/10.1007/s00186-016-0549-x.
V. M. Panaretos, Y. Zemel, Statistical aspects of wasserstein distances, Annual review of statistics and its application 6 (2019) 405–431. doi:https://doi.org/10.1146/annurev-statistics-030718-104938.
C.-C. Ni, Y.-Y. Lin, F. Luo, J. Gao, Community detection on networks with ricci flow, Scientific reports 9 (2019) 9984. doi:https://doi.org/10.1038/s41598-019-46380-9.
E. Angriman, A. van der Grinten, M. Hamann, H. Meyerhenke, M. Penschuck, Algorithms for large-scale network analysis and the networkit toolkit, in: Algorithms for Big Data: DFG Priority Program 1736, Springer Nature Switzerland Cham, 2023, pp. 3–20. doi:https://doi.org/10.1007/978-3-031-21534-6.
C. L. Staudt, A. Sazonovs, H. Meyerhenke, Networkit: A tool suite for large-scale complex network analysis, Network Science 4 (2016) 508–530. doi:https://doi.org/10.1017/nws.2016.20.
F. Kuhn, P. Schneider, Computing shortest paths and diameter in the hybrid network model, in: Proceedings of the 39th Symposium on Principles of Distributed Computing, 2020, pp. 109–118. doi:https://doi.org/10.1145/3382734.3405719.
S. Vaid, R. Salih, R. Gayathri, J. J. Nair, All pair shortest path using distributed architectures, in: 2017 International Conference on Advances in Computing, Communications and Informatics (ICACCI), IEEE, 2017, pp. 2000–204. doi:https://doi.org/10.1109/ICACCI.2017.8126138.
I. Rahayuda, N. Santiari, Dijkstra and bidirectional dijkstra on determining evacuation routes, in: Journal of Physics: Conference Series, volume 1803, IOP Publishing, 2021, p. 012018. doi:https://doi.org/10.1088/1742-6596/1803/1/012018.
G. Vaira, O. Kurasova, Parallel bidirectional dijkstra's shortest path algorithm, Databases and Information Systems VI, Frontiers in Artificial Intelligence and Applications 224 (2011) 422–435.
R. Sreejith, K. Mohanraj, J. Jost, E. Saucan, A. Samal, Forman curvature for complex networks, Journal of Statistical Mechanics: Theory and Experiment 2016 (2016) 063206. doi:https://doi.org/10.1088/1742-5468/2016/06/063206.
Forman, Bochner's method for cell complexes and combinatorial ricci curvature, Discrete & Computational Geometry 29 (2003) 323–374. doi:https://doi.org/10.1007/s00454-002-0743-x.
C.-C. Ni, Y.-Y. Lin, J. Gao, X. Gu, Network alignment by discrete ollivier-ricci flow, in: International symposium on graph drawing and network visualization, Springer, 2018, pp. 447–462. doi:https://doi.org/10.1007/978-3-030-04414-5_32.
R. S. Hamilton, Three-manifolds with positive ricci curvature, Journal of Differential geometry 17 (1982) 255–306. doi:https://projecteuclid.org/journalArticle/Download?urlId=10.4310\%2Fjdg\%2F1214436922.
M. Girvan, M. E. Newman, Community structure in social and biological networks, Proceedings of the national academy of sciences 99 (2002) 7821–7826. doi:https://doi.org/10.1073/pnas.122653799.
J. Takalo, Extracting hale cycle related components from cosmic-ray data using principal component analysis, Solar Physics 297 (2022) 113. doi:https://doi.org/10.1007/s11207-022-02048-8.
H. Koeksal, N. Demir, A. Kilcik, Analysis of the cosmic ray effects on sentinel-1 sar satellite data, Aerospace 8 (2021) 62. doi:https://doi.org/10.3390/aerospace8030062.